

Center for Advanced Materials

# CAM

RECEIVED  
LAWRENCE  
BERKELEY LABORATORY

DEC 5 1989

LIBRARY AND  
DOCUMENTS SECTION

Submitted to Metallurgical Transactions

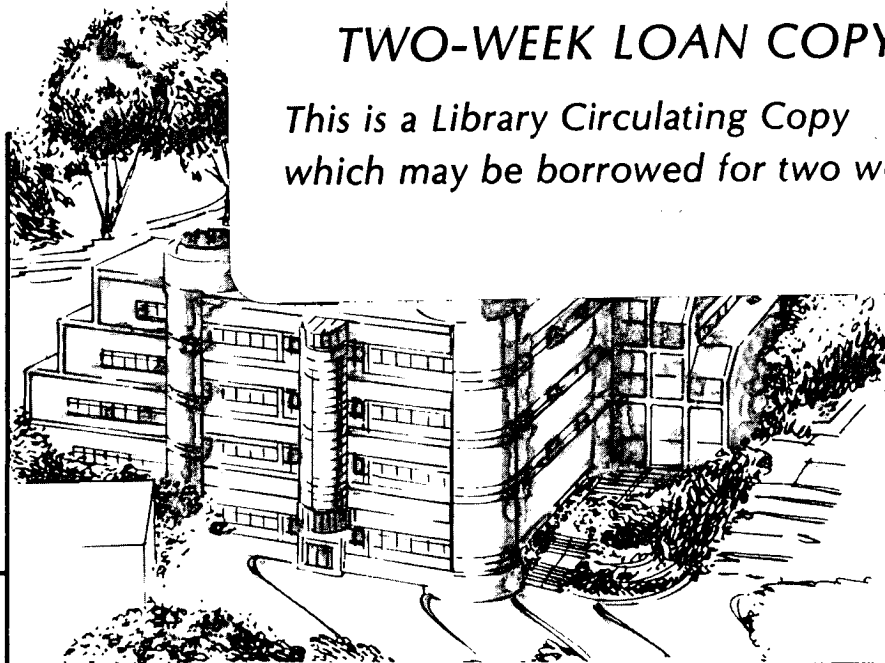
## The Microstructures of Al-Sc Alloys with Ternary Additions

R.R. Sawtell and J.W. Morris, Jr.

June 1989

**TWO-WEEK LOAN COPY**

*This is a Library Circulating Copy  
which may be borrowed for two weeks.*



**Materials and Chemical Sciences Division**

**Lawrence Berkeley Laboratory • University of California**

ONE CYCLOTRON ROAD, BERKELEY, CA 94720 • (415) 486-4755

LBL-27145  
c.2

## **DISCLAIMER**

This document was prepared as an account of work sponsored by the United States Government. While this document is believed to contain correct information, neither the United States Government nor any agency thereof, nor the Regents of the University of California, nor any of their employees, makes any warranty, express or implied, or assumes any legal responsibility for the accuracy, completeness, or usefulness of any information, apparatus, product, or process disclosed, or represents that its use would not infringe privately owned rights. Reference herein to any specific commercial product, process, or service by its trade name, trademark, manufacturer, or otherwise, does not necessarily constitute or imply its endorsement, recommendation, or favoring by the United States Government or any agency thereof, or the Regents of the University of California. The views and opinions of authors expressed herein do not necessarily state or reflect those of the United States Government or any agency thereof or the Regents of the University of California.

**The Microstructures of Al-Sc Alloys with Ternary Additions**

Ralph R. Sawtell and J. W. Morris, Jr.

Center for Advanced Materials  
Materials and Chemical Sciences Division  
Lawrence Berkeley Laboratory  
1 Cyclotron Road  
Berkeley, CA 94720

and

Department of Materials Science and Mineral Engineering  
University of California

June 1989

This work was jointly supported by the Aluminum Company of America, ALCOA Laboratories, and by the Director, Office of Energy Research, Office of Basic Energy Sciences, Materials Science Division of the U. S. Department of Energy under Contract No. *DE-AC03-76SF00098*

# Microstructures of Al-Sc Alloys with Ternary Additions

Ralph R. Sawtell and J. W. Morris, Jr.

Center for Advanced Materials, Lawrence Berkeley Laboratory  
and  
Department of Materials Science and Mineral Engineering  
University of California, Berkeley

The microstructures of a series of ternary, precipitation hardenable Al-Sc-RE alloys have been studied, where Re designates an Y or rare earth addition. The peak strengths of these alloys had been previously found to vary systematically with RE size and increased by as much as 25 percent compared to binary Al-Sc alloys. The microstructural study revealed that these alloys are strengthened by extremely fine  $L1_2$  precipitates and that precipitate chemistry varies in a manner that depends on RE size. It is concluded that modifications in precipitate structure lead to an increase in precipitation strengthening efficiency with RE size that dominates an opposing decrease in precipitate volume fraction.

## I. Introduction

Although they are not yet well known, the benefits of using scandium as an alloying addition to aluminum are substantial, and have been established in a series of investigations at the Alcoa and other research laboratories [1-3]. In particular, Al-Mg alloys with small additions of Sc have excellent combinations of strength, toughness and corrosion resistance at room and cryogenic temperatures together with low density and good superplastic forming capabilities. The principal shortcoming of scandium is its high cost and limited availability. In a previous paper [4] we investigated the use of ternary additions to the Al-Sc binary in an effort to improve the efficiency of precipitation hardening to improve properties or reduce the Sc content needed for a given level of performance. The technical approach was to select ternary additions that would interact with Sc in the  $L1_2$  phase precipitates that are known to form in Al-Sc alloys in an attempt to increase precipitate strength and volume fraction. Yttrium and the lanthanide rare earth elements were selected as candidates because of their chemical similarity to Sc.

In the work reported in Ref. [4] four Al-Sc-RE alloys and an Al-Sc binary control were cast, fabricated and tested. The RE additions were Er, Ho, Gd and Y, and the alloys had the same nominal composition, Al-0.3Sc-0.3RE, in atom percent. It was found that peak tensile strength increased monotonically with the RE atom size, and improved substantially over that of the Al-0.3Sc control. The peak strength of Al-0.3Sc was increased by more than 20% by the addition of Y or Gd. Differential scanning calorimetric studies led to the conclusion that only one strengthening precipitate formed, and resistivity measurements indicated that peak strength was reached at smaller precipitate sizes as the RE

size increased. These results are consistent with the hypothesis that the RE elements are incorporated into the L<sub>12</sub> Al-Sc precipitate and increase its strength at given size. However, the work reported in [4] did not include detailed microstructural studies and therefore did not clarify the relative contributions of changes in the precipitate strength, the precipitate volume fraction, and other microstructural features to the strength increment of the alloy. This information is particularly relevant to the further development of Al-Sc-X alloys since the theoretical analysis presented in [4] suggests that as the size of the ternary RE element increases, it should improve the hardening efficiency of the L<sub>12</sub> precipitate, but should be incorporated into it in a lesser fraction, which decreases the precipitate volume fraction and the attainable precipitate strength. The balance of these factors determines the optimum hardening element and alloy composition.

A microstructural and microchemical analysis of ternary Al-Sc-RE alloys was therefore undertaken. The results are reported below.

## II. Materials and Experimental Procedure

The Al-Sc-RE alloys chosen for this study are listed in Table I. As discussed in ref. [4] the RE additions were selected to provide a systematic variation in atom size. Equal atom fractions of Sc and the RE were used and the Sc content was held constant. The concentration of the ternary addition was chosen in the expectation that it would exceed the constrained L<sub>12</sub> solubility limit for the larger-sized ternary additions, but not for the smaller ones, and would hence allow study of the balance between the expected increase in the hardness of the L<sub>12</sub> precipitate with RE size and the concomitant decrease in the solubility of the RE element in the precipitate, which determines the total precipitate strength and the volume fraction of precipitate that will form. The alloys were cast from pure starting materials into chilled copper crucibles after melting in an MgO crucible in an air furnace. They were then machined into cylindrical specimens and cold drawn into 0.44 mm. wire. Further experimental details regarding the casting and fabrication, and precise compositions of the alloys are given in ref. [4].

Table I: Alloy Compositions

System	RE Radius (nm)	Composition, at. pct. (wt. pct.)				
		Sc	Er	Ho	Gd	Y
Al-Sc	--	0.3 (0.5)				
Al-Sc-Er	0.1757	0.3 (0.5)	0.3 (1.8)			
Al-Sc-Ho	0.1765	0.3 (0.5)		0.3 (1.8)		
Al-Sc-Gd	0.1801	0.3 (0.5)			0.3 (1.7)	
Al-Sc-Y	0.1802	0.3 (0.5)				0.3 (1.0)

The microstructural studies done in this work included X-ray diffraction, optical microscopy, scanning electron microscopy (SEM) and transmission electron microscopy (TEM). Microchemical analysis was done with analytic electron microscopy (STEM).

X-ray diffraction was used for the structural analysis of the phases formed during solidification and aging. Samples for x-ray diffraction were prepared by chemical thinning to ~ 0.1 mm using a solution of concentrated HCl and water with an NiSO<sub>4</sub> catalyst.

Analyses were made with a Guinier-deWolfe camera in the transmission configuration employing monochromatic Cu radiation. Diffraction patterns were recorded on film. Line positions were then digitized and lattice spacing calculated using a calibration function for this radiation type and geometry.

Scanning electron microscopy was used to obtain information on the grain and sub-grain structure of the fabricated specimens as well as their crystallographic texture. The method used for analyzing substructure was somewhat unusual and relies on channeling enhanced contrast in the backscattered mode [5]. The microscope used was a JEOL JSM 840A operating at 7KV. Samples were prepared by electropolishing using an electrolyte containing 23 pct. concentrated nitric acid in methanol maintained at  $-30^{\circ}\text{C}$ . Samples were electropolished for 1.5 min. at 8 volts. Mean grain intercept lengths were determined by digitizing boundary intersections along a series of randomly oriented lines. Texture was determined using the same instrument employing electron backscatter patterns (EBSP). This technique [6] employs backscatter Kikuchi diffraction at high incident angle to give very localized information on crystallographic orientation. An accelerating voltage of 14KV was used for the EBSP work.

Transmission and scanning transmission electron microscopy were used to determine the configuration and composition of the strengthening precipitates. A variety of specialized techniques and microscopes were used during the investigation including Philips EM301, EM400T and EM420T machines as well as the Atomic Resolution Microscope (ARM) at the National Center for Electron Microscopy (NCEM). The EM301 was operated at 100 kV and used for general examinations while the EM400 and EM420T were operated at 120 kV and used primarily for analytical electron microscopy. KEVEX and EDAX energy dispersive x-ray spectrometers were installed on these instruments. Theoretical K-factors were used in both cases. Absorption effects were considered but found to be insignificant. The ARM was used for high resolution studies of precipitates in the peak aged condition. This instrument was operated at 800 KV. HREM simulations and optical diffraction analyses were also carried out at NCEM. Simulations were constructed using the NCEMSS package [7] employing parameters appropriate for the ARM.

Standard electrochemical techniques were used for sample preparation in all cases. An electrolyte containing 23 pct.  $\text{HNO}_3$  in methanol at  $-30^{\circ}\text{C}$  was used in a Struers Tenupol 2 electropolishing unit with an average sample potential of 18 volts. These condition produced an average current density of about  $3 \text{ A/cm}^2$ .

### III. Results

#### *Optical Metallography*

Optical micrographs of the as-cast samples and cross sections of the fabricated wires are presented in Figures 1 and 2 for the Al-Sc and Al-Sc-Gd alloys, respectively, as examples of the microstructures observed. Because of rapid solidification, the microstructures of the ingot samples were quite fine. The solidification cell size varied from 12 to 15  $\mu\text{m}$ , which is consistent with a cooling rate of approximately  $50^{\circ}\text{C}/\text{sec}$ . [8]. Relatively few intermetallic particles appear in the Al-Sc ingot (Figure 1a) but a pronounced cellular eutectic microstructure is evident in the cast ternary alloys as shown in Figure 2a for the Al-Sc-Gd alloy. This microstructure is not surprising since the concentrations of the ternary additions exceed their equilibrium solubilities in aluminum.

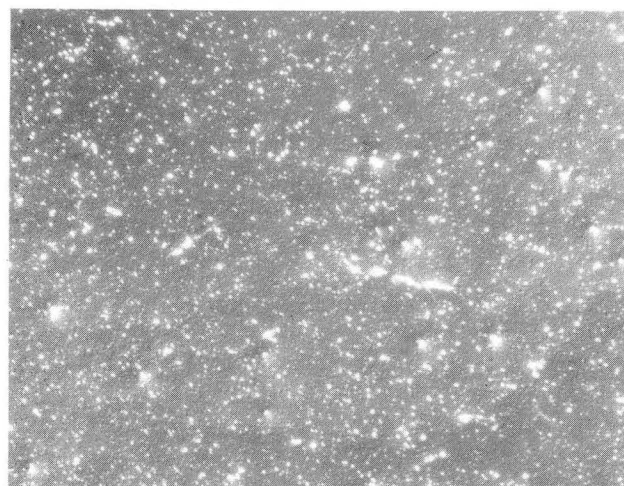
The micrographs of the drawn wire samples (Figures 1b and 2b) show that the distribution of intermetallic phases is well refined by the extensive cold working employed in fabrication. Again, relatively fewer particles are observed in the Al-Sc alloy (Fig. 1b). The cellular structure observed in the ternary alloy ingot was completely eliminated by the cold working operation as illustrated by the micrograph of the Al-Sc-Gd alloy wire presented in Figure 2b.

### Guinier X-ray Diffraction

Cold worked and aged samples were prepared for Guinier X-ray diffraction analysis to determine the nature of the coarse phases formed during solidification. This technique would be expected to be relatively insensitive to precipitated phases in these systems because of fine particle sizes. Indeed, no measurable differences were noted among aged and unaged samples. A summary of the phases detected appears in Table II.

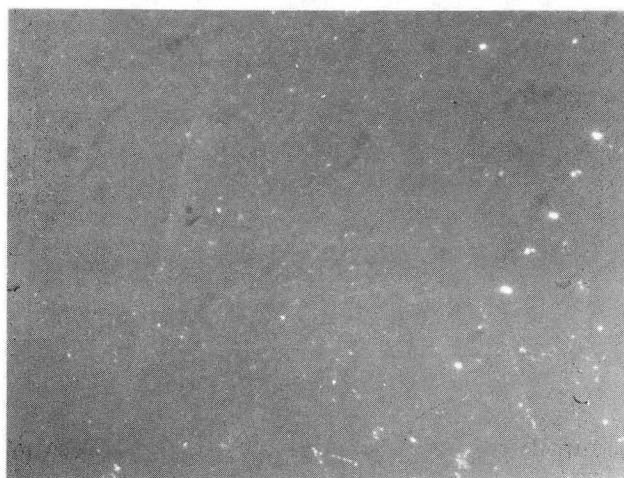
**Table II: Intermetallic Phases Present in Cold Rolled and Aged Al-Sc-(RE) Alloys**

Alloy	Structure Type			Al <sub>12</sub> Gd <sub>2</sub>
	Al	Cu <sub>3</sub> Au	Pb <sub>3</sub> Ba	
Al-Sc	X	X		
Al-Sc-Y	X	X	X	
Al-Sc-Gd	X	X	X	X
Al-Sc-Ho	X	X		
Al-Sc-Er	X	X		



(a)

50  $\mu\text{m}$

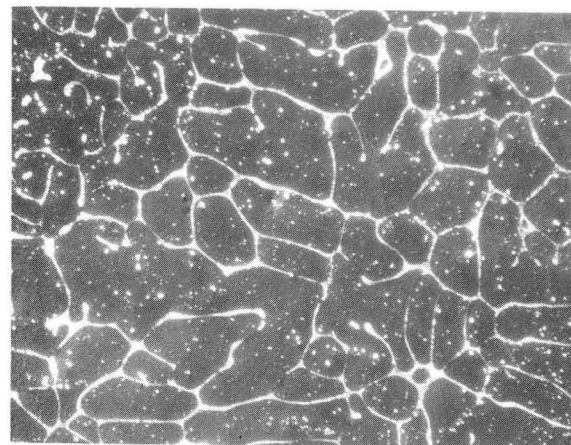


(b)

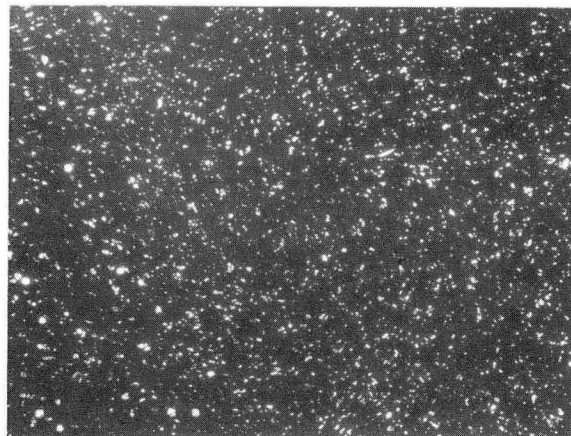
50  $\mu\text{m}$

XBB880-9971

Figure 1. Optical micrographs of Al-Sc ingot (a) and drawn wire (b).  
(polarized light with differential interference contrast)



(a)

50  $\mu\text{m}$ 

(b)

50  $\mu\text{m}$ 

XBB880-9970

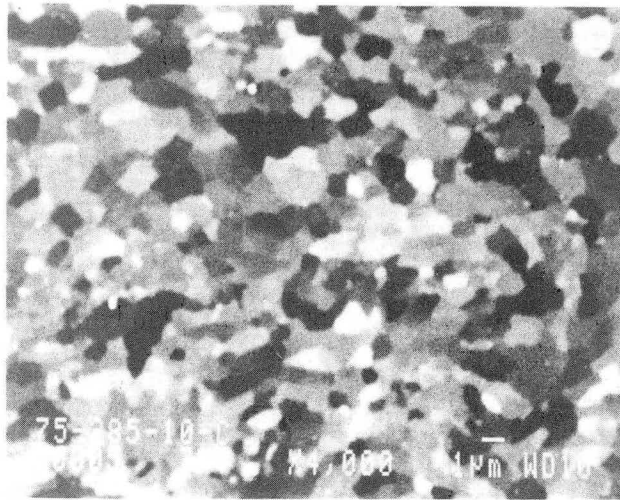
Figure 2. Optical micrographs of Al-Sc-Gd ingot (a) and drawn wire (b). (polarized light with differential interference contrast)

The actual compositions of the phases detected in the ternary alloys could not be determined by the X-ray data alone but it is quite likely that the  $L1_2$  phase, for example, contains both Sc and the RE. It should also be noted that the  $Pb_3Ba$  type structure is not observed at equilibrium in binary Al-Y and Al-Gd intermetallics [1,2].

#### *Scanning Electron Microscopy*

Although transmission electron microscopy is often used to evaluate grain structure, channeling enhanced backscattered contrast in the SEM allows sampling of a much greater area and, thus, provides better counting statistics. Samples of the wire material were examined using this technique for a variety of artificial aging temperatures and at a number of locations along the wire radius. All examinations were done on faces perpendicular to the

wire drawing axis. As an example of the images produced by channeling enhanced backscattered contrast, a micrograph of the Al-Sc alloy wire is provided in Figure 3. The detail produced is reminiscent of that produced in optical metallography when using polarized light on specimens that have been electropolished.

5  $\mu\text{m}$ 

XBB880-9972

Figure 3. Scanning electron micrograph of Al-Sc alloy wire obtained with channeling enhanced backscattered electron contrast.

Because small differences in grain size can have appreciable influence on strength, the SEM images were analyzed quantitatively. The measure of grain size used was linear grain boundary intercept length which, for idealized grain shape, can be translated to grain diameter through a multiplicative factor of 1.68. The distribution of intercept lengths was approximately log-normal and no significant difference in boundary intercept length was observed between samples of a given alloy aged at temperatures ranging from 235 to 310°C. Grain boundary intercept length was also constant across the wire diameter.

The mean and most probable grain boundary intercept lengths are shown for the various alloys in Table III. Given the available data for the Hall-Petch constants for aluminum alloy wire [9-12], we can calculate the substructure contribution to strengthening. The results are also given in Table III. Very little difference is observed in the average grain intercept length, from which we conclude that differences in the grain size had very little effect on alloy strength ( $\Delta\sigma \leq 6$  MPa).

A limited study of grain boundary misorientation was also done in the SEM using EBSP. The vast majority of the grain boundaries are apparently high-angle boundaries (>5-10 deg.). This is not surprising since deformation in alloys with little strain hardening is known to be very nonuniform with a preponderance of slip bands and resultant severe local lattice rotations. Since there is little if any true recrystallization in these alloys, the recovered subgrain structure is representative of this deformation structure.

Table III: Grain Size Data for Al-Sc-(RE) Alloy Wires

Alloy	Average Grain Intercept Length ( $\mu\text{m}$ )	Most Probable Grain Intercept Length ( $\mu\text{m}$ )	Calculated* Strength (MPa)
Al-Sc	1.001	0.8	109.9
Al-Sc-Y	1.054	0.7	105.6
Al-Sc-Gd	1.058	0.75	105.3
Al-Sc-Ho	1.034	0.75	107.2
Al-Sc-Er	1.081	1.05	103.6

\* Calculated using data in reference 4

### Transmission Electron Microscopy

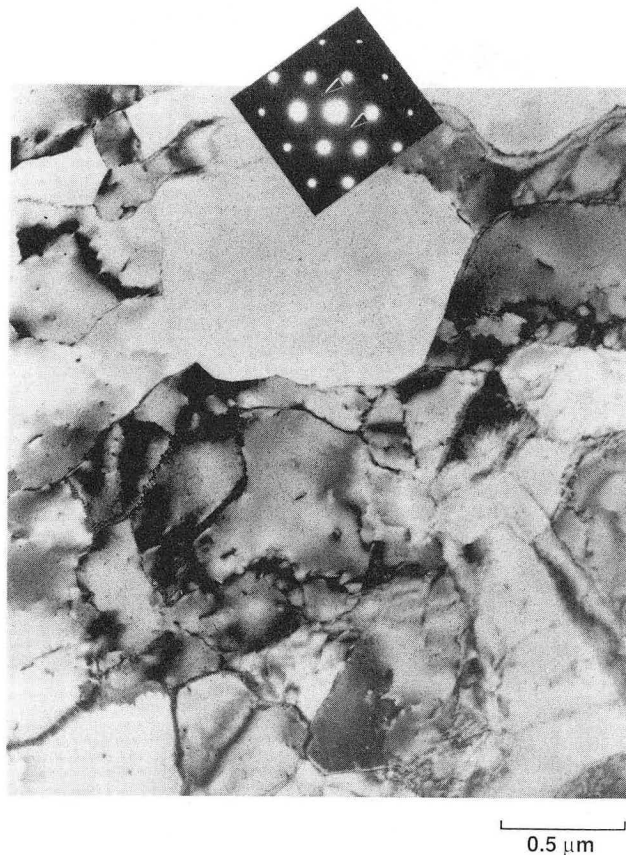
Transmission electron microscopy was used to characterize the chemical and structural nature of the  $L_{12}$  precipitates in the alloys studied. The microstructures in the peak aged condition were studied using conventional TEM techniques. In addition, overaged samples were examined using analytical electron microscopy (STEM) and the peak aged microstructures were investigated using high resolution electron microscopy (HREM). The results obtained will be presented in this order.

Samples of each of the alloys in the peak aged condition were examined using conventional TEM. Although quantitative analysis of grain and subgrain size was not attempted, qualitative observations were in agreement with the SEM results presented in the previous section. A representative micrograph showing the general microstructure is presented in Figure 4 along with a selected area diffraction pattern obtained from the center of this area. As shown in this figure, the grain boundaries are quite irregular and not at all reminiscent of the equilibrium grain structure of pure aluminum. This is due to the pinning effects of the  $L_{12}$  precipitates. Although the precipitates are not readily visible at this level of resolution, the diffraction pattern shown in Figure 4 includes the  $L_{12}$  superlattice reflections. Isolated dislocations can also be observed but not in sufficient quantities to significantly alter alloy properties.

Because precipitates in the peak aged condition were found to be too small to analyze using conventional STEM techniques, samples of each alloy were overaged to coarsen the precipitates on the assumption that their composition would vary no more than slightly with size so long as they remained coherent. A soak of 1 hour duration at 450°C was used for this purpose. As shown in Figure 5, the general appearance of the microstructure of these alloys was not greatly altered by the overaging treatment. The  $L_{12}$ ,  $Al_3(\text{Sc,RE})$  precipitates still remain effective barriers to grain boundary migration. After the soaking treatment the precipitate size was of the order of 30 nm for all of the alloys. Qualitative analysis of the strain field contrast using 2-beam imaging conditions indicated that the precipitates remained coherent after coarsening. As expected, the strain fields are interstitial in nature (particle lattice parameter larger than matrix).

The analysis of the precipitate compositions employed standard analytic techniques for energy dispersive spectrometry (EDS). In analytic microscopy work there is always a trade-off between spatial resolution and the EDS count rate, which determines the accuracy of the chemical analysis. In this case, the minimum probe size that would afford an ac-

ceptable count rate (based on sample drift, contamination, etc.) was slightly larger than the average size of the particles to be analyzed. Because of this, and the fact that the particles were generally contained within the foil, some matrix was included in each analysis. Thus, the absolute values of Sc and RE recorded could not be used directly. Instead, ratios of Sc to RE based on atomic percentages were used. Between 8 and 10 particles were analyzed for each alloy. Analyses of the matrix composition were also recorded and in all cases Sc and RE levels were below detectable limits.



XBB880-10010

Figure 4. Bright field TEM micrograph showing the general microstructure of an Al-Sc-Ho alloy in the peak aged condition. Selected area diffraction pattern for the central region of this area is also shown.



XBB880-10011

Figure 5. Bright field TEM micrograph showing the general microstructure of an Al-Sc-Gd alloy in the overaged condition. A selected area diffraction pattern for the central region of this area is also shown.

The average values of the Sc/RE composition ratio measured in the  $L_{12}$  precipitates, along with the limits of a 95 pct. confidence interval are shown in Table IV. Fractions of RE in the  $Al_3(Sc_{1-x}RE_x)$  phase (i.e., the value of  $x$ ) were calculated from these values and are shown, along with the experimentally determined bulk values [13,14] in Table V. The measured composition is plotted as a function of the ternary RE radius in Figure 6. To clarify these results, it should be pointed out that the limit of substitution of RE in the  $L_{12}$  phase is 0.5 for the RE concentrations used here, if all of the Sc is incorporated in the  $L_{12}$  precipitates. Metallographic and X-ray results presented earlier show that some of the ternary RE are gathered into the large incoherent phases formed during solidification, which reduces the total amounts available to the  $L_{12}$  precipitates. Hence it is possible that the measured RE substitution in the Al-Sc-Ho and Al-Sc-Er alloys is influenced more by the limited RE availability than by the coherent phase equilibrium. Taking into account the inconsistency in the bulk Al-Sc-Y data noted in our previous paper, the results for RE sub-

stitution in the Al-Sc-Gd and Al-Sc-Y alloys are remarkably close to the values that would be anticipated from bulk data.

**Table IV: Sc/RE Composition Ratio for Coherent Precipitates in Al-Sc-RE Alloys**

Alloy	Sc/RE Composition Ratio		
	Mean	95 Pct. Conf. Int.	
		Upper	Lower
Al-Sc-Er	2.56	3.47	1.66
Al-Sc-Ho	2.05	2.71	1.39
Al-Sc-Y	3.93	5.01	2.85
Al-Sc-Gd	4.83	5.59	4.07

**Table V: Calculated Fraction RE in  $Al_3(Sc_{1-x}RE_x)$  Precipitates**

Alloy	RE Radius (nm)	RE Substitution			
		Precipitate			Bulk
		Mean	Upper	Lower	
Al-Sc-Er	0.1757	0.294	0.364	0.224	0.90
Al-Sc-Ho	0.1765	0.335	0.394	0.275	0.72
Al-Sc-Y	0.1800	0.211	0.249	0.173	0.60
Al-Sc-Gd	0.1801	0.175	0.198	0.152	0.15

Although electron diffraction had already indicated the presence of an  $L1_2$  precipitate phase in each of the alloys, HREM was used to determine the configuration of the precipitates in the peak aged condition.

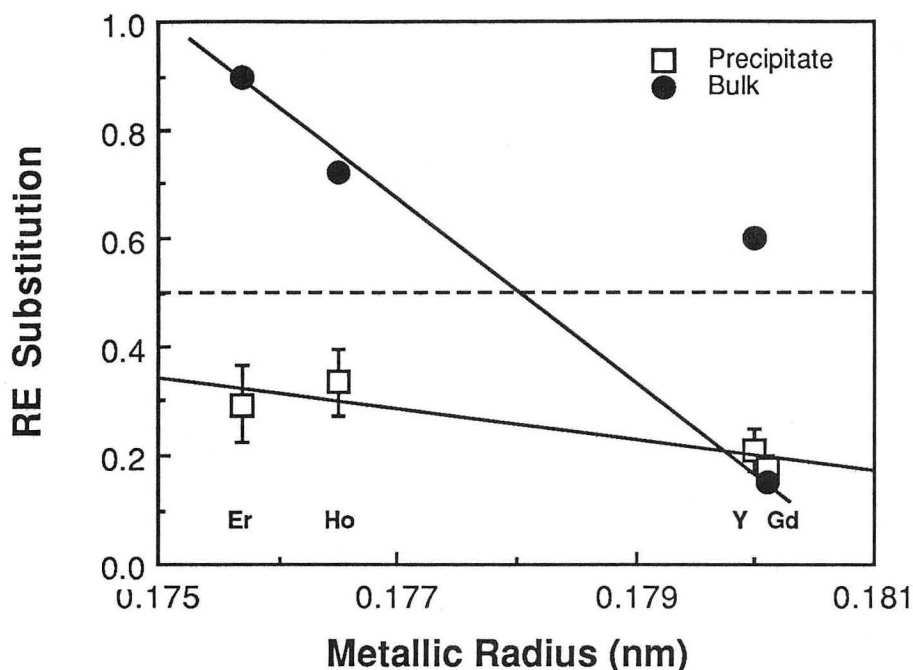
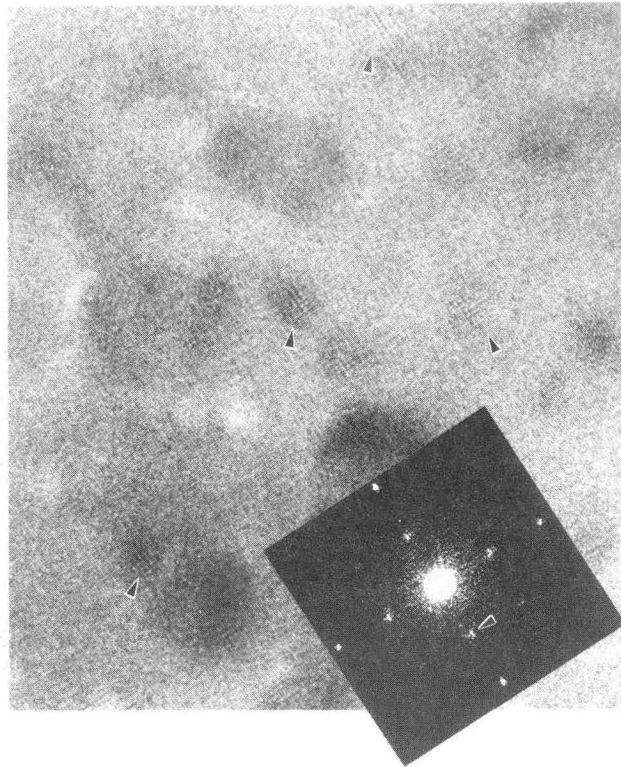


Figure 6. Re substitution as a function of RE metallic radius for bulk and precipitated  $\text{Al}_3(\text{Sc}_{1-x}\text{RE}_x)$  phases. Note that in both cases substitution increases with decreasing RE radius.

A key adjunct to experimental HREM is the simulation of phase contrast images via digital computer. In cases where complex structures are to be analyzed, simulation is vital for determining causal correlation between proposed structures and recorded images. In the case of simple structures, like the  $\text{L}_{12}$  phase of interest in this work, simulations are perhaps most useful in defining imaging conditions that provide the best contrast between the matrix and precipitate phases. For any given microscope the most common imaging variables are specimen orientation, thickness and objective lens defocus. As far as orientation is concerned, the  $[001]$  zone is a convenient choice for this system because only the  $\{002\}$  matrix and  $\{001\}$   $\text{L}_{12}$  superlattice reflections need be considered. Simulations for thin foils in this zone showed that contrast between matrix and precipitate was better for relatively large values of objective lens defocus.

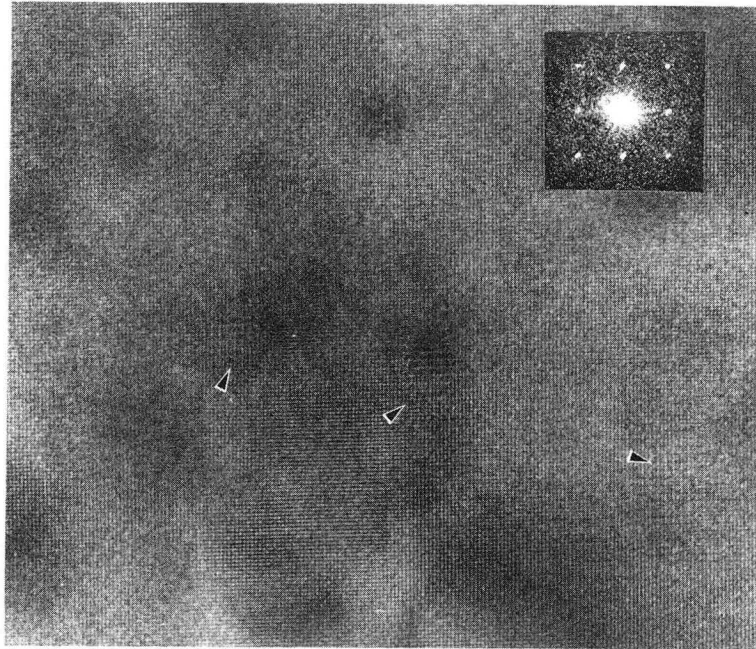
Precipitates were imaged in the peak aged condition and representative micrographs showing the precipitate shapes and distributions for the Al-Sc-Gd (highest strength, lowest RE substitution) and Al-Sc-Ho (lowest strength, highest RE substitution) alloys are presented in Figures 7 and 8. An example of a larger particle detected in the Al-Sc-Ho alloy with more defined superlattice fringes is shown in Figure 9. In each of the figures, optical diffraction patterns [15] are provided to show the structure of the precipitate phase relative to that of the Al matrix. An aperture corresponding to  $\sim 12$  nm at the sample plane was used to obtain these patterns. The precipitate patterns all show the characteristic superlattice reflections of the  $\text{L}_{12}$  phases which were absent in the matrix patterns. Image simulations for the microscope conditions used provided additional evidence that the precipitates are of the  $\text{L}_{12}$  type.

Although several areas of each sample were viewed and imaged, this is far too little information to provide a *statistically valid* average precipitate size or spacing. Qualitatively, however, the distribution of precipitates appears uniform with an average diameter of 3 nm for both alloys.



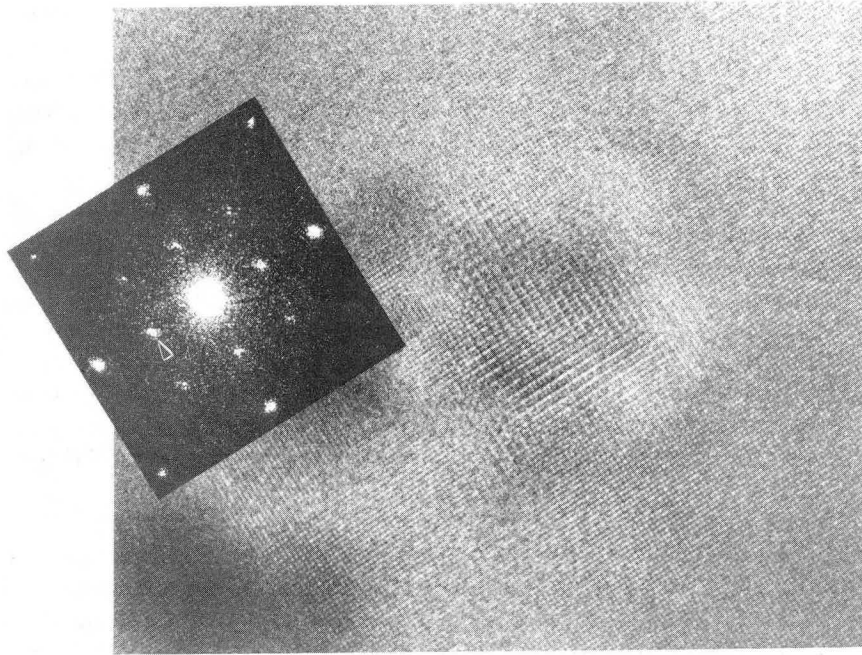
XBB880-10012

Figure 7. HREM micrograph showing  $L1_2$  precipitates (lattice fringe doubling) in a peak aged Al-Sc-Ho alloy. Matrix fringe spacing is 0.2025 nm. Precipitates are  $\cong 15$  fringe spacing or 3 nm in diameter. ([001] zone)



XBB880-10623

Figure 8. HREM micrograph showing L<sub>12</sub> precipitates (lattice fringe doubling) in a peak aged Al-Sc-Gd alloy. Matrix fringe spacing is 0.2025 nm. Precipitates are  $\cong 15$  fringe spacing or 3 nm in diameter. ([001] zone)



XBB880-10013

Figure 9. HREM micrograph showing a larger  $L_{12}$  precipitate in a peak aged Al-Sc-Ho alloy. Matrix fringe spacing is 0.2025 nm. ([001] zone)

#### IV. Discussion

The present work was undertaken to characterize the volume fraction, structure, shape, and chemical composition of the hardening precipitates in Al-Sc-RE alloys in order to determine the source of the strength improvement documented in ref. [4]. As shown by optical metallography and X-ray phase analysis, the RE concentrations in the Al-0.3Sc-0.3RE alloys tested were in excess of the solubility limit hence coarse phases were formed during solidification. This occurred despite attempts to suppress these reactions by using mildly rapid solidification. As a result, the concentrations of ternary elements in solution and available for precipitation were not the same for the various alloys. This complicates, but does not preclude an analysis of the different behavior of the various RE elements.

First we consider possible variations in substructure and solid solution strengthening. Since the grain size did not vary significantly between alloys, substructure hardening is eliminated as a cause of the variations in peak strength. In principle, solid solution strengthening could be a factor because solution hardening should increase with RE size. The failure to detect alloying elements in solution by analytic microscopy is not definitive since the minimum detectable mass of RE, of the order of 0.1-0.3 weight percent [16], is of the same order as the ternary atom content. However, the small quantity of the ternary addition makes it unlikely that solution strengthening could be responsible for strengthening effects of the magnitude observed. We therefore conclude that the observed differences in strength are due to precipitation hardening.

Four characteristics of the distribution of hardening precipitates may change with the ternary addition: the precipitate structure, shape, volume fraction and composition. These factors together determine the quantitative degree of precipitation hardening. The precipitate structure and shape are apparently the same for the Al-Sc-RE alloys investigated here; only spherical,  $L1_2$  precipitates were observed. However, the results suggest that the composition and volume fraction changes significantly.

The precipitate compositions estimated from the results of analytic microscopy are given in Tables IV and V. The precipitate volume fractions can be estimated from this data under the assumption that all of the Sc is incorporated into precipitates. The results are shown in Table VI along with values of the peak tensile strength. Table VI also contains values of the precipitate lattice parameter, which are estimated on the basis of the measured composition and the known lattice parameters of the ternary intermetallics in bulk. As mentioned previously, the increase in RE substitution with decreasing RE size is consistent with the published information on the solubility of RE in ternary Al-Sc-RE intermetallics.

The results presented in Table VI show that the maximum tensile strength varies inversely with the estimated volume fraction. We therefore conclude that the precipitate volume fraction is not the controlling variable; the dominant factor appears to be the effective strength of the precipitate phase. This conclusion is consistent with the results of resistivity studies given in ref. [4], which appear to show that the peak strength occurs at smaller precipitate sizes as the alloy strength increases.

**Table VI: Calculated Precipitate Lattice Parameters and Volume Fractions**

Alloy	RE Radius (nm)	RE Substitution	Lattice Parameter (nm)	Volume Fraction (pct.)	Peak Strength (MPa)
Al-Sc	--	0	0.4583	1.20	251
Al-Sc-Er	0.1757	0.294	0.4697	1.70	278
Al-Sc-Ho	0.1765	0.335	0.4720	1.80	262
Al-Sc-Y	0.1800	0.211	0.4690	1.52	290
Al-Sc-Gd	0.1801	0.175	0.4673	1.45	309

Given the conclusion that the increase in alloy strength with RE size is due to the higher inherent strength of the precipitate phase, we now consider how the "strength" of the  $L1_2$  phase changes with the RE radius. The strength of the precipitate is its resistance to the passage of a dislocation. As discussed in ref. [4], an increase in strength at given precipitate size and shape is most likely associated with one of two changes: (1) an increase in the coherency strain associated with the precipitate, which increases its interaction with a dislocation, or (2) an increase in the energy of an anti-phase boundary within the precipitate, which increases the force required to move a dislocation through it.

The first possibility can be evaluated from the measured precipitate composition. Calculated lattice parameters for the precipitate phases are presented in Table VI. These data show relatively little variation and little or no correlation to the peak strength values. If anything, the trend is opposite to the data; higher misfit is associated with lower strength. Thus, an increase in the precipitate strain does not appear to be the dominant factor.

The possibility that the anti-phase boundary energy increases with RE size is more plausible, and, in fact, is indicated by the results of differential scanning calorimetry (DSC) on these alloys that were given in ref. [4]. Fig. 3 of ref. [4] shows that the heat of precipitation measured by DSC increases sharply with the RE radius. Fig. 8 of ref. [4] shows that the variation is very nearly the same as the change of alloy strength with RE radius. Since the heat of precipitation depends on the volume fraction of precipitates as well as on their thermodynamic stability, the data in ref. [4] does not by itself show that the molar enthalpy of the precipitate phase increases with RE size. However, the results obtained in this work suggest that the volume fraction decreases slightly with RE size. It, hence, seems clear that the stability of the  $L_{12}$  phase with respect to the Al solid solution increases with RE size. Since, at least to first order, the anti-phase boundary energy of an ordered intermetallic compound increases with the enthalpy of formation, the DSC results suggest a monotonic increase in anti-phase boundary energy with RE size.

Assuming order hardening, an increase in the anti-phase boundary energy raises the precipitate strength at given size, that is, it increases the "hardening efficiency" of the precipitate phase. As the hardening efficiency increases, the peak strength increases, and occurs at smaller precipitate size. While the results obtained here are not definitive and other factors may contribute, the results of this investigation strongly suggest that the increase in strength of Al-Sc-RE alloys with RE size is due to the influence of the RE element on the anti-phase boundary energy of the ordered  $L_{12}$  precipitates.

The results of this investigation also suggest useful approaches to the design of viable Al-Sc alloys. Alloys containing Y or Gd in addition to Sc were shown to develop strengths 50-60 MPa higher than the binary Al-Sc control. This is a useful increment in performance that could help make commercial variants of these alloys containing solid solution strengtheners like Mg and or Li quite competitive. From a practical point of view, Y may be the best choice of the ternary additions studied here because of its greater equilibrium solubility, lower density and relatively lower cost. Given appropriate processing, however, Gd additions produce the highest strength.

## V. Conclusion

The characterization studies reported confirm that Al-Sc-RE alloys (RE = Er, Ho, Y or Gd) are precipitation-hardened by an  $L_{12}$  hardening precipitate like the  $Al_3Sc$  precipitate found in the Al-Sc binary. The RE elements are incorporated into the  $L_{12}$  precipitate to a degree that decreases with the RE size. The principal effect of the RE incorporation appears to be an increase in the anti-phase boundary energy of the hardening precipitate. The anti-phase boundary energy, whose qualitative behavior is inferred from the heat of formation, increases with the RE radius. It is apparently responsible for the significant increase in hardness with RE size.

### Acknowledgement

This research was jointly supported by the Aluminum Company of America, ALCOA Laboratories, and by the Director, Office of Energy Research, Office of Basic Energy Sciences under Contract No. DE-AC03-76SF00098. All HREM work was conducted at The National Center for Electron Microscopy at the Lawrence Berkeley Laboratory.

### References

1. L. A. Willey, *U.S. Patent 3,619,181*, 1971.
2. R. R. Sawtell and C. L. Jensen, *Met. Trans. A*, 1989, In Press.
3. S. L. Verzasconi, Masters Thesis, University of California, Berkeley, 1989.
4. R. R. Sawtell and J. W. Morris, Jr., *Met Trans. A*, 1989, In Press.
5. H. J. McQueen and W. B. Hutchinson, *Deformation of Polycrystals*, RISO National Laboratory, Roskilde, Denmark, 1981, pp 335-342.
6. D. J. Dingley, M. Longden, J. Weinbren and J Alderman, *Scanning Electron Microscopy*, 1984, vol. 2, pp 569-575.
7. R. Kilaas, *Proc. EMSA* , 1987, pp 66-69.
8. *Aluminum*, Ed. J. E. Hatch, ASM, 1984.
9. N. Hansen, *Met. Trans. A*, 1985, vol. 16A, pp 2167-2190.
10. S. K. Varma and B. G. LeFevre, *Met. Trans. A*, 1980, vol.11A, pp 935-941.
11. D. J. Lloyd and D. Kenny, *Acta Met.*, 1980, vol. 28, pp 639-649.
12. D. Kalish and B. G. LeFevre, *Met. Trans. A*, 1975, vol. 6A, pp 1319-1324.
13. O. I. Zalutskaya, V. G. Kontsevov, N. I. Karamyshev, V. R. Ryabov and I. I. Zalutsky, *Dop. Akad. Nauk. Ukrain. RSR [A]*, 1970, vol. 8, pp 751-753.
14. O. I. Zalutskaya, V. R. Ryabov and I. I. Zalutsky, *Dop. Akad. Nauk. Ukrain. RSR [A]*, 1970, vol. 3, pp 255-259.
15. R. Sinclair, R. Gronsky and G. Thomas, *Acta Met.* , 1976, vol. 24, pp 789-796.
16. D. B. Williams, *Practical Analytical Electron Microscopy in Material Science*, Verlag, 1984.

LAWRENCE BERKELEY LABORATORY  
CENTER FOR ADVANCED MATERIALS  
1 CYCLOTRON ROAD  
BERKELEY, CALIFORNIA 94720